Quantum networking with short-range entanglement assistance

Siddhartha Santra ⬤ and Vladimir S. Malinovsky ⬤

U.S. Army Research Laboratory, Adelphi, Maryland 20783, USA

We propose an approach to distribute high-fidelity long-range entanglement in a quantum network assisted by the entanglement supplied by auxiliary short-range paths between the network nodes. Entanglement assistance in the form of shared catalyst states is utilized to maximize the efficiency of entanglement concentration transformations over the edges of the network. The catalyst states are recycled for use in adaptive operations at the network nodes and replenished periodically using the auxiliary short-range paths. The rate of long-range entanglement distribution using such entanglement assistance is found to be significantly higher than possible without using entanglement assistance.

I. INTRODUCTION

Long-range entanglement in a quantum network [1] enables promising applications ranging from unconditionally secure communications [2] and loophole-free tests of quantum nonlocality [3] to a network of quantum clocks [4] and quantum-enhanced interferometry [5]. The entanglement generated initially in such networks is short range, that is, in the form of entangled states on edges between neighboring nodes. Subsequently, long-range entanglement may be obtained between two remote nodes by identifying a path over the primary entangled edges and connecting them via entanglement swapping operations [6] at the intermediate nodes such as in the quantum repeater [7] approach.

A quantum network should be seen as more than an interlaced collection of linear quantum repeaters. The latter utilize local quantum operations at the network nodes aided by classical communication (LOCC), such as filtration [8] or entanglement distillation [9], to distribute entanglement over long distances. Yet, existing repeater protocols do not fully exploit the entanglement along auxiliary short-range paths between the nodes of the network that may be afforded, for example, by a dynamic topology [10], heterogenous links involving different degrees of freedom of the flying qudits [11], or load sharing in the quantum data plane of the network [12]. The inefficient utilization of short-range entanglement in a quantum network hinders high-fidelity long-range entanglement distribution where modest rates limit the quantum advantage of the potential applications.

In this work we propose an approach to efficiently utilize short-range entanglement assistance for high-fidelity long-range entanglement distribution in a quantum network. Here, auxiliary short-range paths supply catalyst states shared between network nodes that enable a transformation of the entanglement assisted local operations and classical communication (ELOCC) class [13]. This class of operations allows more general entanglement transformations in the network than LOCC. We utilize a catalytic ELOCC transformation

(catalysis) to concentrate the entanglement content of primary low-fidelity states on network edges with a higher success probability compared to LOCC. Hence, a small number of the primary states are required to obtain a state with a high fidelity to a Bell state that is necessary for long-range entanglement distribution.

Catalysis is a one-shot procedure and if it succeeds the catalyst state is recovered intact along with the desired Bell state creation. The same catalyst state may be reused up to an expected number of times determined by the catalysis success probability. If the procedure fails, no Bell state is obtained and the catalyst state is lost as well. For sustained long-range entanglement distribution the primary states are continuously generated over the edges along the path connecting the remote nodes in a quantum repeaterlike manner. Whereas, the stock of catalyst states needs to be replenished only periodically using the auxiliary short-range paths between neighboring nodes allowed by the topology of the network (see Fig. 1).

Our approach therefore goes beyond the linear repeater paradigm and establishes a way of quantumly aggregating the entanglement resources provided by short-range paths in a quantum network. Together with its resource-efficient and one-shot feature, this can significantly enhance the long-range entanglement distribution rate between remote nodes in the network compared to when no auxiliary short-range entanglement assistance is available.

The paper is organized as follows. In Sec. II we describe the theory of entanglement catalysis. Next, in Sec. III we describe the model for the network edges, catalytic transformations over the network edges, and the rate of remote entanglement distribution in the network. We conclude with a summary of the results and open questions in Sec. IV.

II. ENTANGLEMENT CATALYSIS

In catalysis, two parties at network nodes A and B utilize a shared entangled pure state $|\mathcal{C}\rangle$ (the catalyst) to achieve certain entanglement transformations forbidden using only
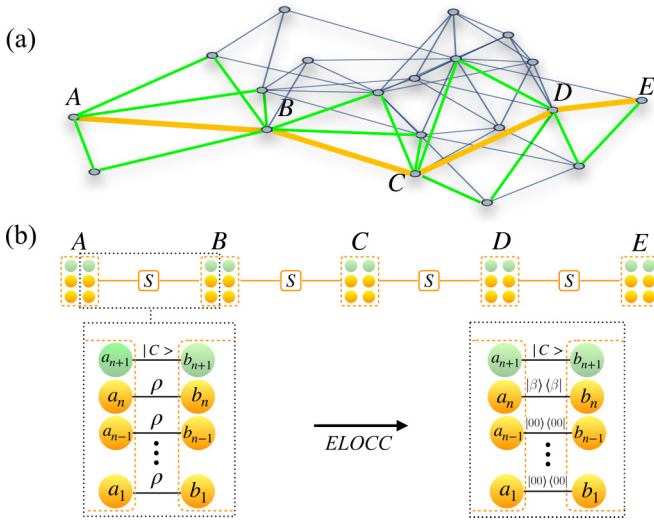
FIG. 1. (a) Schematic of a quantum network. Yellow-colored edges comprise the long-range entanglement distribution path connecting remote nodes A and E. Green-colored edges show available auxiliary short-range paths between neighboring nodes. (b) An ELOCC based long-range entanglement distribution path. Neighboring half-nodes share n copies of a state ρ on qubit pairs $(a_i, b_i)_{i=1}^{i=n}$ (yellow spheres) and a catalyst state $|C\rangle$ stored on the qubit pair (a_{n+1}, b_{n+1}) (green spheres).

LOCC [14]. Rather than being consumed, the catalyst state is recovered after the transformation, i.e.,

$$\sigma \underset{\text{LOCC}}{\nrightarrow} \rho$$

$$\sigma \otimes |\mathcal{C}\rangle \langle \mathcal{C}| \underset{\text{LOCC}}{\rightarrow} \rho \otimes |\mathcal{C}\rangle \langle \mathcal{C}|, \tag{1}$$

where σ, ρ, $|\mathcal{C}\rangle$ are bipartite states shared by A and B. More generally, catalysis can increase the success probability of even some probabilistic entanglement transformations compatible with LOCC [15]. The set of possible catalysts for a desired transformation can be determined from the Schmidt coefficients of the initial and final states [13]. For certain pairs of pure states, $\sigma = |\psi\rangle \langle\psi|$ and $\rho = |\phi\rangle \langle\phi|$, a catalyst enabling a deterministic transformation, i.e., with $P_{\text{cat}}(I \rightarrow F) = 1$, from an initial state $|I\rangle = |\psi\rangle |\mathcal{C}\rangle$ to a final state $|F\rangle = |\phi\rangle |\mathcal{C}\rangle$ can be found. This is possible if and only if the entanglement monotones [15], $E_k(X) := 1 - \sum_{j=0}^{k-1} \lambda_k^X$, $X = I, F$, that are functions of the ordered Schmidt coefficients, $\bar{\lambda}^X = (\lambda_1^X \geqslant \lambda_2^X \geqslant \cdots \geqslant \lambda_d^X)$, of the initial and final states are nonincreasing,

$$E_k(I) \geqslant E_k(F) \quad \forall k \in [1, d], \tag{2}$$

where d is the larger among the dimensions of the initial and final states.

For some pairs of $|\psi\rangle$, $|\phi\rangle$ no catalyst can make the transformation $|I\rangle \rightarrow |F\rangle$ deterministic, i.e., $P(I \rightarrow F) \neq 1$, but can still increase the success probability as compared to just LQCC, i.e., $P_{\text{cat}}(I \rightarrow F) > P(\psi \rightarrow \phi)$ [16]. The success probability in this case is given by

$$P_{\text{cat}}(I \rightarrow F) = \min_{1 \leqslant k \leqslant d} R_k(I, F), \tag{3}$$

where $R_k(I, F) := E_k(I)/E_k(F)$, $k \in [1, d]$ is the ratio of the entanglement monotones of the initial and final states. In general, catalysts fulfilling the inequality in Eq. (2) or maximizing the right-hand side of Eq. (3) can be easily obtained using linear programming techniques [17]. Catalysis has been shown to be more powerful than LOCC also for the case when σ and ρ are genuinely mixed states [18], although no straightforward criteria such as the inequality in Eq. (2) exists in this case.

Pure state probabilistic catalysis is already sufficient, however, to boost the long-range entanglement distribution rate in a quantum network with assistance from the entanglement along auxiliary short-range paths. We illustrate this in a case where both the primary and catalyst states are two-qubit entangled states, although in general they may have different dimensions. We first motivate the form of the primary states generated on the network edges followed by a description of the catalysis process assuming availability of the catalyst. The model of the communication channel over the network edges accounts for polarization-dependent losses (PDL) in the channel which is an important mechanism affecting the quality of the distributed remote entangled states as demonstrated by much current interest in strategies [19–21] to mitigate PDL. We then discuss how to obtain the said catalysts and demonstrate the enhancement that entanglement assistance obtained via auxiliary short-range paths can provide to the long-range entanglement distribution rate.

III. ENTANGLEMENT DISTRIBUTION USING SHORT-RANGE ENTANGLEMENT ASSISTANCE

A. Polarization-dependent losses over the network edges

Consider a source, S, of polarization entangled photon pairs on an edge A-B along a path connecting two remote nodes A and E in a quantum network as shown in Fig. 1. S produces photon pairs in the state, $|\psi^+\rangle = (|HV\rangle + |VH\rangle)/\sqrt{2}$, which travel through the connecting optical fibers of length, L_0, to heralded quantum memories, e.g., [22], at A and B. However, due to PDL in the fiber and other connecting elements the state vector of a single qubit in a superposition state undergoes the transformation, $\zeta_0 |H\rangle + \zeta_1 |V\rangle \rightarrow \zeta_0(\sqrt{t_H} |H\rangle + \sqrt{1 - t_H} |0\rangle) + \zeta_1 |V\rangle$. That is, a horizontally polarized photon gets effectively mixed with the vacuum mode at a beamsplitter with transmittivity $0 < t_H < 1$, whereas a vertically polarized photon suffers no relative loss. The state of the two quantum memories conditioned on heralding, which we assume occurs with probability P_0, is therefore $\rho = |\alpha\rangle \langle\alpha|$ with

$$|\alpha\rangle = \sqrt{\alpha} |HV\rangle + \sqrt{1 - \alpha} |VH\rangle, \tag{4}$$

where $\alpha = t_H^L/(t_H^L + t_H^R)$ and $t_H^{L,R}$ are the transmittivities of the left and the right channels relative to the source. In general, since $\alpha \neq (1/2)$, the primary entanglement is in the form of partially entangled states of fidelity, $F_{L_0}(\rho) = |\langle\psi^+|\alpha\rangle|^2 = \frac{1}{2} + \sqrt{\alpha(1 - \alpha)} < 1$.

A direct utilization of the states ρ of the form in Eq. (4) to obtain a long-range entangled state, ρ_{AE}, via entanglement swapping at intermediate nodes using Bell state measurements and corrective unitaries based on the measurement results, leads to a rapid decrease of the expected fidelity of ρ_{AE}.

Assuming primary entanglement generation over each edge as described above, the expected fidelity of ρ_{AE} approaches the distillability threshold exponentially fast with the total length, i.e., $\langle \psi^+ | \rho_{AE} | \psi^+ \rangle - \frac{1}{2} \sim [\alpha(1-\alpha)]^{N/2}$, where $N = L_{\text{tot}}/L_0$ is the number of edges along the path. Since much higher temporal resources are required for the entanglement manipulation of lower fidelity states to obtain a high-fidelity state, the rate of directly obtaining the latter over long range is greatly suppressed. The fidelity of the entangled states over each edge therefore needs to be enhanced before the entanglement connections are made in order to achieve a reasonable long-range entanglement distribution rate.

B. Catalytic entanglement transformations over the network edges

An optimal catalytic transformation can efficiently provide Bell states over the network edges utilizing a few copies of the state ρ and one copy of a nonmaximally entangled catalyst, $|\mathcal{C}\rangle = \sqrt{c} |HV\rangle + \sqrt{1-c} |VH\rangle$, $0.5 < c < 1$. For this, at least $(n+1)$-qubit quantum memories are required at each half-node so that n copies of the state ρ and one copy of the catalyst shared with the neighboring node are available for implementing the transformation,

$$\rho^{\otimes n} \otimes |\mathcal{C}\rangle \langle \mathcal{C}| \rightarrow |\beta\rangle \langle \beta| \otimes |00\rangle \langle 00|^{\otimes(n-1)} \otimes |\mathcal{C}\rangle \langle \mathcal{C}|, \quad (5)$$

with $|\beta\rangle = (|HV\rangle + |VH\rangle)/\sqrt{2}$. The transformation concentrates the entanglement in n copies of the partially entangled state ρ into a single maximally entangled state $|\beta\rangle$ in a two-step process using adaptive unitary operations and measurements dependent on the parameters α and c and one round of two-way classical communication between the nodes [14,15] and is probabilistic in general [16] (see Appendix B).

In step one, a temporary shared state $|\gamma(n, \alpha, c)\rangle$ is deterministically obtained via a sequence of operations on the initial joint state, $|\alpha\rangle^{\otimes n} |\mathcal{C}\rangle$, of qubits at A and B. The entries of $|\gamma(n, \alpha, c)\rangle$ can be obtained algorithmically from the set of ratios, $R_l(I, F)$, $l \in [1, 2^{n+1}]$, and the entanglement monotones, $E_l(F)$, for the initial and final states given by the left- and right-hand sides of the transformation in Eq. (5), respectively. Essentially, $|\gamma(n, \alpha, c)\rangle$ is a state that maximizes the success probability in Eq. (5) achievable using only local measurements at either node. In step two, a generalized measurement with two outcomes is performed at one of the nodes on its portion of $|\gamma(n, \alpha, c)\rangle$. Corresponding to one of the measurement outcomes the state $|\beta\rangle \otimes |00\rangle^{\otimes(n-1)} \otimes |\mathcal{C}\rangle$ is successfully obtained with probability $P_{\text{cat}}^{\max}(n, \alpha, c)$. The success (or failure) of the measurement is then relayed to the other node. In the case of success, agents at A and B can utilize the shared state $|\beta\rangle$ for entanglement swapping to extend its range (if the adjacent edges on either side also report success) and the catalyst state for further local entanglement concentration operations. Whereas, in the case of failure they restart the process of generating n copies of $|\alpha\rangle$ and reobtaining the catalyst, $|\mathcal{C}\rangle$.

The success probability $P_{\text{cat}}^{\max}(n, \alpha, c)$ of the transformation in Eq. (5) increases with n for fixed α and c, that is, for a given initial state and choice of catalyst. However, generating and storing more copies of ρ is temporally and spatially expensive. Further, the depth of the quantum circuit to imple-

ment the above steps at each network node scales as $\sim 2^{n+1}$. Therefore, in a quantum network catalytic transformations that require collective manipulations of a smaller number of qubits are desirable. At least two copies of ρ are required for any catalyst to boost $P_{\text{cat}}^{\max}(n, \alpha, c)$, compared to the optimal LOCC success probability $P_{\text{LOCC}}^{\max}(n, \alpha) = 2(1-\alpha^n)$ of the transformation $\rho^{\otimes n} \rightarrow |\beta\rangle \langle \beta| \otimes |00\rangle \langle 00|^{\otimes(n-1)}$. Whereas, for a large number of copies, $n \geqslant n_*(\alpha)$, where $n_*(\alpha) := \lceil 1/\log_2(1/\alpha) \rceil$, $\alpha \in [0.5, 1)$, catalysis is not needed as in that case the same transformation can be achieved with certainty using LOCC without any catalyst. Accessing just a few copies of the primary entangled states in the range $n \in \{2, \ldots, [n_*(\alpha) - 1]\}$, and utilizing the optimal two-qubit catalyst $|\mathcal{C}_{\text{opt}}(n, \alpha)\rangle = \sqrt{c_0(n, \alpha)} |HV\rangle + \sqrt{1 - c_0(n, \alpha)} |VH\rangle$, the probability $P_{\text{cat}}^{\max}(n, \alpha, c_0) = (1 - \alpha^n)/[1 - c_0(n, \alpha)]$ can be significantly higher than $P_{\text{LOCC}}^{\max}(n, \alpha)$. To quantify the increase in efficiency due to catalysis, we define $\eta_P(n, \alpha, c) := P_{\text{cat}}^{\max}(n, \alpha, c)/P_{\text{LOCC}}^{\max}(n, \alpha)$. This ratio diverges when the optimal two-qubit catalyst is used in Eq. (5) for poor quality primary entangled states, that is, $\eta_P(n, \alpha, c) \sim 1/\sqrt{n}\sqrt{(1-\alpha)}$, for $c = c_0(n, \alpha)$ and as $\alpha \rightarrow 1$.

The catalyst state itself can be obtained from the resources provided by the primary and auxiliary paths between the relevant nodes (A, B in our case). It may be obtained deterministically using a LOCC procedure if the paths provide pure states that satisfy the criteria given by the inequality in Eq. (2), or else it may be obtained only probabilistically. For example, in our case, it turns out that the optimal two-qubit catalyst $|\mathcal{C}_{\text{opt}}(n, \alpha)\rangle$ in Eq. (5) is completely determined by α and n with its Schmidt coefficient given by $c_0(n, \alpha) = \{1 + 3\alpha^n - [(1 + 3\alpha^n)^2 - 16\alpha^{2n}]^{1/2}\}/4\alpha^n$, $n \geqslant 2$. Therefore, it suffices to use n_{cat} copies of $|\alpha\rangle$, where $\alpha^{n_{\text{cat}}} \leqslant c_0(n, \alpha)$, in order to implement $|\alpha\rangle^{\otimes n_{\text{cat}}} \rightarrow |\mathcal{C}_{\text{opt}}(n, \alpha)\rangle$, with certainty using LOCC—if the only resources available are the primary entangled states ρ. Note that the minimum number of copies needed to obtain the catalyst is determined by n and α since $n_{\text{cat}}(n, \alpha) \geqslant \lceil \log_2 [c_0(n, \alpha)]/\log_2(\alpha) \rceil$.

If auxiliary paths $i = 1, \ldots, \mathcal{N}_{\text{aux-path}}$, each supplying states $|\alpha^{(i)}\rangle$ between the nodes are available, then $n_{\text{cat}}^{(i)} \geqslant \lceil \log_2 [c_0(n, \alpha)]/\log_2(\alpha^{(i)}) \rceil$, copies of the states are respectively enough to obtain a single copy of $|\mathcal{C}_{\text{opt}}(n, \alpha)\rangle$. The resources provided by distinct paths can also be combined to obtain the catalyst. For example, a subset of states with different multiplicities among the $|\alpha^{(i)}\rangle$ can provide the catalyst deterministically if their product $\prod_i |\alpha^{(i)}\rangle^{\otimes m_i}$, $m_i \in \mathbb{N}$ satisfies the inequality in Eq. (2) relative to $|\mathcal{C}_{\text{opt}}(n, \alpha)\rangle$. Of course, more general catalysts (other than the optimal) [16] may also be used for entanglement manipulation over the network edges—the choice depends on the tradeoff between the temporal resources expended to obtain the catalyst and the entanglement distribution rate.

C. Rate of remote entanglement distribution in the network

The average temporal resource needed for every catalysis attempt over a network edge is the statistical average of the temporal resources needed for success and failure events, i.e.,

$$\langle T_{L_0} \rangle = P_{\text{cat}}^{\max} \langle T_{\text{pri}} \rangle + \left(1 - P_{\text{cat}}^{\max}\right) \langle T_{\text{pri+cat}} \rangle, \quad (6)$$

where $\langle T_{\mathrm{pri}} \rangle$ and $\langle T_{\mathrm{pri+cat}} \rangle$ are the average times to obtain the primary entangled states and the primary entangled states along with the catalyst, respectively. We assume that the primary entanglement generation takes much longer than the local operation time at the nodes, which is typically the case. The terms on the right-hand side of Eq. (6) also depend on several parameters as we now explain. The catalysis success probability $P_{\mathrm{cat}}^{\mathrm{max}}(n, \alpha, c)$ clearly depends on the number of copies, the primary entangled state, and the choice of catalyst via n, α, c. Next, since the time to success of an entanglement generation attempt is geometrically distributed, we obtain $\langle T_{\mathrm{pri}} \rangle = n(T_0/P_0)$, where $T_0 = 2L_0/c_f$, with c_f the speed of light in the fiber, and P_0 are the average time required and probability for primary entanglement generation.

The behavior of $\langle T_{\mathrm{pri+cat}} \rangle$ depends on the availability of auxiliary short-range paths between nodes A and B. If the catalyst states are supplied exclusively by the auxiliary paths, then $\langle T_{\mathrm{pri+cat}} \rangle = \max\{\langle T_{\mathrm{pri}} \rangle, \langle T_{\mathrm{cat}} \rangle\}$ is the larger among the primary entanglement generation time and the catalyst generation time. With $\mathcal{N}_{\mathrm{aux\text{-}path}}$ auxiliary paths, for each of which $P_i, T_i, n_{\mathrm{cat}}^{(i)}$ are the entanglement generation probability, entanglement generation time, and number of states required to obtain the catalyst, respectively, we obtain $\langle T_{\mathrm{cat}} \rangle = 1/\sum_i (n_{\mathrm{cat}}^{(i)} P_i / \langle T_i \rangle) \leqslant 1/\mathcal{N}_{\mathrm{aux\text{-}path}} \min_i (n_{\mathrm{cat}}^{(i)} P_i / \langle T_i \rangle)$. In the limit of a large number of auxiliary paths, $\mathcal{N}_{\mathrm{aux\text{-}path}} \gg 1$, the temporal resource needed to generate the catalyst is less than the primary entanglement generation time, $\langle T_{\mathrm{cat}} \rangle \leqslant \langle T_{\mathrm{pri}} \rangle$, therefore $\langle T_{\mathrm{pri+cat}} \rangle = \langle T_{\mathrm{pri}} \rangle$. This is effectively the case when the auxiliary paths can supply the catalyst faster than they are consumed due to failure events which occur with an average time of $\langle T_{\mathrm{pri}} \rangle / (1 - P_{\mathrm{cat}}^{\mathrm{max}})$. In the other limit, when there are no auxiliary paths available, $\mathcal{N}_{\mathrm{aux\text{-}path}} = 0$, in which case the temporal resource needed to obtain the catalysts is budgeted from the primary entanglement generation process. Thus, in this limit the overhead of temporal resource needed is additive, $\langle T_{\mathrm{pri+cat}} \rangle = \langle T_{\mathrm{pri}} \rangle + \langle T_{\mathrm{cat}} \rangle = [n + n_{\mathrm{cat}}(n, \alpha)]T_0/P_0$.

The rate of long-range entanglement distribution in a quantum network along a path where the edges use optimal catalysis for entanglement concentration can be calculated as

$$R_{\mathrm{cat}}^{(N)}(n, \alpha, c) = \frac{1}{\langle T_{L_0} \rangle Z^{(N)}\big[P_{\mathrm{cat}}^{\mathrm{max}}(n, \alpha, c)\big]}, \qquad (7)$$

where $Z^{(N)}(P) = \sum_{j=1}^{N} \binom{N}{j} \frac{(-1)^{j+1}}{1-(1-P)^j}$ [23] is the waiting time [24] to obtain successful events in all of the N edges that comprise the path of length, NL_0. On the other hand, in a quantum network where the edges utilize the optimal LOCC procedure to obtain Bell states, the rate is given by $R_{\mathrm{LOCC}}^{(N)}(n, \alpha) = 1/\langle T_{\mathrm{pri}} \rangle Z^{(N)}[P_{\mathrm{LOCC}}^{\mathrm{max}}(n, \alpha)]$. Note that both the rates, $R_{\mathrm{cat}}^{(N)}(n, \alpha, c)$ and $R_{\mathrm{LOCC}}^{(N)}(n, \alpha)$, are independent of the final fidelity (which is 1) but depend on the fidelity of the primary entangled states through α.

The ratio of the two rates, $\eta_R^{(N)}(n, \alpha, c) := R_{\mathrm{cat}}^{(N)}(n, \alpha, c)/R_{\mathrm{LOCC}}^{(N)}(n, \alpha)$, estimates the enhancement due to short-range entanglement assistance in the network. It is especially amplified when the primary entangled states are of poor quality and the optimal catalyst is used in the transformation in Eq. (5), that is, as $\alpha \to 1$ and $c = c_0(n, \alpha)$ (see Fig. 2). In this limit, when no auxiliary paths are available the ratio of rates approaches
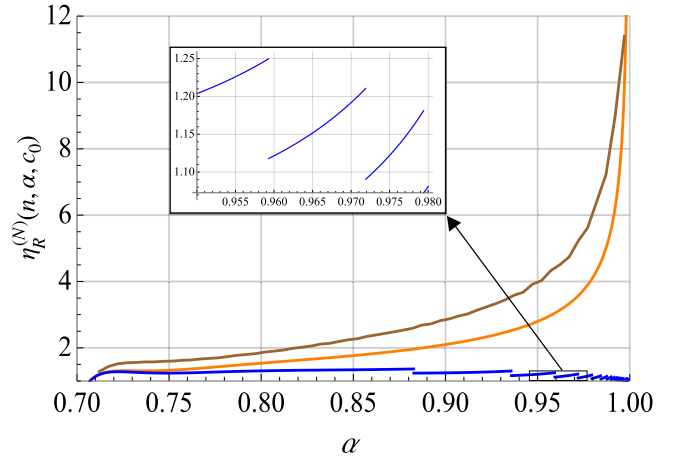

FIG. 2. Ratio of long-range entanglement distribution rate using optimal catalysis to the rate using optimal LOCC for the transformation in Eq. (5) with $n = 2$ on $N = 2^5$ edges along a network path. The brown (upper) curve shows the ratio using the optimal catalyst of Hilbert space dimension 4×4 whereas the middle (orange) curve shows the same ratio using the optimal catalyst of Hilbert space dimension 2×2 when, $\mathcal{N}_{\mathrm{aux\text{-}path}} \gg 1$. The blue (lower, discontinuous) curve shows the ratio with the optimal 2×2 catalyst for $\mathcal{N}_{\mathrm{aux\text{-}path}} = 0$. Inset shows the nature of discontinuity; it occurs whenever the number of copies of the primary entangled state needed to obtain the catalyst jumps by 1.

$\eta_R^{(N)}(n, \alpha, c_0) \to (\langle T_{\mathrm{pri}} \rangle / \langle T_{\mathrm{cat}} \rangle) \eta_P(n, \alpha, c_0) \approx 1$. This is because the temporal overhead to generate the catalysts diminishes the advantage in rate due to the increase in the entanglement concentration success probability through catalysis. Whereas, in the same limit, $\alpha \to 1$, when a large number of auxiliary paths are available the ratio diverges, $\eta_R^{(N)}(n, \alpha, c_0) \to \eta_P(n, \alpha, c_0) \sim 1/\sqrt{n}\sqrt{(1-\alpha)}$, for paths of arbitrary length. In Fig. 2, the marginal enhancement observed in the $\mathcal{N}_{\mathrm{aux\text{-}path}} = 0$ and $\alpha \nrightarrow 1$ regime (blue line) is due to the fact that catalytic entanglement concentration involves the collective manipulation of a slightly larger number of qubits in each attempt, making it a bit more efficient.

IV. CONCLUSIONS

We have shown that catalysis based long-range entanglement distribution in a quantum network works particularly well under resource limited conditions, when only a small number of copies of poor quality primary entangled states are available. Its advantage is contingent upon many auxiliary short-range paths providing the catalysts. In this approach the spatial and temporal resources needed at the network nodes are constant with respect to the total length of the path, and the long-range entanglement is obtained in the form of high-fidelity maximally entangled Bell states. We also note that the identification of suitable catalysts and design of the adaptive quantum circuit required for the catalytic transformation can be fully automated using classical computational resources at the nodes given an estimate of the primary entangled states.

In a quantum network, catalysis can enhance or enable more general entanglement transformations beyond the pure state case since mixed state entanglement transformations can

also be catalyzed [18]. This is relevant when the decoherence of the primary entangled states during storage or processing at the nodes is taken into account. However, mixed state catalysis does not improve the purification efficiency in the case in which the decohered states are modeled as Werner states [25]. For other models of decoherence, where the final state is not a Werner state, an interesting direction for further research is to the understand the advantage that catalysis can provide for output states of quantum channels relevant for long-range entanglement distribution, e.g., the depolarizing and dephasing channels [26]. In the future we will further address the following questions: (1) Can catalysis be useful when only partial state information is available? (2) Can catalysis be used in networks to efficiently distribute multiparty entangled states, such as the Greenberger-Horne-Zeilinger or W states [27]?

We believe the results obtained here will stimulate research on the above mentioned questions and can facilitate developments in long-range entanglement distribution necessary for the future quantum internet.

APPENDIX A: STEPS FOR CATALYTIC ENTANGLEMENT CONCENTRATION

We first summarize the two steps needed to implement the transformation in Eq. (5) of the main text.

In step one, a temporary shared state $|\gamma(n, \alpha, c)\rangle$ which majorizes the initial state $|\alpha\rangle^{\otimes n} |\mathcal{C}\rangle$ is obtained with unit probability via operations on the joint state of qubits, $\{a_i\}_{i=1}^{i=(n+1)}$ and $\{b_i\}_{i=1}^{i=(n+1)}$, at A and B, corresponding to a sequence of at most $n_T \leqslant (2^{n+1} - 1) \, T$ transforms [14] (e.g., $n_T = 5$ for $n = 2$). The entries of $|\gamma(n, \alpha, c)\rangle$ are obtained algorithmically [15] from the set of ratios, $R_l(I, F), l \in [1, 2^{n+1}]$, and the entanglement monotones of the final state, $E_l(F)$, and are known to the agents at both A and B. A circuit of depth $\sim 20 n_T$ comprising Toffoli, CNOT, single-qubit gates, and single-qubit computational-basis measurements, implements the operations corresponding to the successive T transforms on two-dimensional subspaces of the $(n + 1)$-qubit Hilbert space, $\otimes_{i=1}^{i=(n+1)} \mathcal{H}_{a_i}$, at node A. The set of measurement results is then conveyed as n_T bits of classical data, $\bar{m}_A \in \{0, 1\}^{n_T}$, to the agent at B which determines the unitary it applies, $U_B(\alpha, c, \bar{m}_A)$. The latter can be implemented as a product of unitaries on the corresponding two-dimensional subspaces of $\otimes_{i=1}^{i=(n+1)} \mathcal{H}_{b_i}$, as a quantum circuit of depth $\sim 10 n_T$ using the same set of basic gates. This completes the first step of deterministically obtaining $|\gamma(n, \alpha, c)\rangle$.

In step two, the agent at B performs a two-outcome, $m_{1,2}$, set of generalized measurements, $M_{B,1}(\alpha, c)$ and $M_{B,2}(\alpha, c)$, on its portion of $|\gamma(n, \alpha, c)\rangle$ and obtains the state $|\beta\rangle \otimes |00\rangle^{\otimes(n-1)} \otimes |\mathcal{C}\rangle$ if outcome m_1 is obtained, which occurs with probability $P_{\text{cat}}^{\max}(n, \alpha, c)$. The success (or failure) of the transformation is then relayed to the agent at A via a single bit of classical communication. In the case of success, agents at A and B can utilize the shared state $|\beta\rangle$ for entanglement swapping to extend its range (if the adjacent edges on either side also report success) and the catalyst state for further local entanglement concentration operations. Whereas, in the case of failure they restart the process of generating n copies of $|\alpha\rangle$ and reobtaining the catalyst state, $|\mathcal{C}\rangle$.

APPENDIX B: OPERATIONS FOR CATALYTIC ENTANGLEMENT CONCENTRATION

Here we demonstrate the local operations required at the network nodes for catalytic entanglement concentration using $n = 2$ copies of the primary entangled states $\rho = |\alpha\rangle \langle \alpha|$ and one copy of the optimal two-qubit catalyst state, $|\mathcal{C}_{\text{opt}}(2, \alpha)\rangle$, in Eq. (5) of the main text. We have derived the form of the optimal two-qubit catalyst for general "n" elsewhere [16]; for $n = 2$ it is given by $|\mathcal{C}_{\text{opt}}(2, \alpha)\rangle = \sqrt{c_0(2, \alpha)} |HV\rangle + \sqrt{1 - c_0(2, \alpha)} |VH\rangle$, with $c_0(2, \alpha) = \{1 + 3\alpha^2 - [(1 + 3\alpha^2)^2 - 16\alpha^4]^{1/2}\}/4\alpha^2$. The forms of the unitaries and measurement operators follow from results in [14,15].

All operations at neighboring nodes A, B are performed on two-dimensional subspaces of three qubits at each of the nodes. We use the binary code for the tensor product basis of states on qubits a_1, a_2, a_3 and similarly for b_1, b_2, b_3, therefore,

$$
\begin{aligned}
|000\rangle_{A_1 A_2 A_3} &\to |1\rangle_A, \\
|001\rangle_{A_1 A_2 A_3} &\to |2\rangle_A, \\
|010\rangle_{A_1 A_2 A_3} &\to |3\rangle_A, \\
|011\rangle_{A_1 A_2 A_3} &\to |4\rangle_A, \\
|100\rangle_{A_1 A_2 A_3} &\to |5\rangle_A, \\
|101\rangle_{A_1 A_2 A_3} &\to |6\rangle_A, \\
|110\rangle_{A_1 A_2 A_3} &\to |7\rangle_A, \\
|111\rangle_{A_1 A_2 A_3} &\to |8\rangle_A.
\end{aligned}
\tag{B1}
$$

The state $|\alpha\rangle^{\otimes 2} |\mathcal{C}_{\text{opt}}(2, \alpha)\rangle$ in this basis is then given by the vector (suppressing the arguments of c_0 hereafter),

$$
|I\rangle = |\alpha\rangle^{\otimes 2} |\mathcal{C}_{\text{opt}}(2, \alpha)\rangle =
\begin{pmatrix}
\sqrt{\alpha^2 c_0} \\
\sqrt{\alpha^2 (1 - c_0)} \\
\sqrt{\alpha(1 - \alpha) c_0} \\
\sqrt{\alpha(1 - \alpha) c_0} \\
\sqrt{\alpha(1 - \alpha)(1 - c_0)} \\
\sqrt{\alpha(1 - \alpha)(1 - c_0)} \\
\sqrt{(1 - \alpha)^2 c_0} \\
\sqrt{(1 - \alpha)^2 (1 - c_0)}
\end{pmatrix}.
\tag{B2}
$$

The temporary state $|\gamma[2, \alpha, c_0(2, \alpha)]\rangle$ is given by

$$
|\gamma\rangle =
\begin{pmatrix}
\sqrt{\alpha^2 c_0} \\
\sqrt{\alpha^2 (1 - c_0)} \\
\sqrt{(1 - \alpha^2)/2} \\
\sqrt{(1 - \alpha^2)/2} \\
0 \\
0 \\
0 \\
0
\end{pmatrix},
\tag{B3}
$$

whose Schmidt coefficients majorize those of the initial state.

Step one, as described in the main text, involves a sequence of five T transforms to deterministically obtain $|\gamma\rangle$ from $|I\rangle$ via the following transformations:

$$
|I\rangle \overset{T_{7\text{-}8}^{(1)}}{\to} |I_1\rangle \overset{T_{6\text{-}7}^{(2)}}{\to} |I_2\rangle \overset{T_{5\text{-}6}^{(3)}}{\to} |I_3\rangle \overset{T_{4\text{-}5}^{(4)}}{\to} |I_4\rangle \overset{T_{3\text{-}5}^{(5)}}{\to} |\gamma\rangle,
\tag{B4}
$$

where the four intermediate states $|I_1\rangle \prec |I_2\rangle \prec |I_3\rangle \prec |I_4\rangle$ which sequentially majorize the preceding state are as follows:

$$
\begin{array}{cccc}
|I_1\rangle & |I_2\rangle & |I_3\rangle & |I_4\rangle \\[4pt]
\begin{pmatrix}
\sqrt{\alpha^2 c_0} \\
\sqrt{\alpha^2 (1-c_0)} \\
\sqrt{\alpha(1-\alpha)c_0} \\
\sqrt{\alpha(1-\alpha)c_0} \\
\sqrt{\alpha(1-\alpha)(1-c_0)} \\
\sqrt{\alpha(1-\alpha)(1-c_0)} \\
\sqrt{(1-\alpha)^2 c_0} \\
0
\end{pmatrix},
&
\begin{pmatrix}
\sqrt{\alpha^2 c_0} \\
\sqrt{\alpha^2 (1-c_0)} \\
\sqrt{\alpha(1-\alpha)c_0} \\
\sqrt{\alpha(1-\alpha)c_0} \\
\sqrt{\alpha(1-\alpha)(1-c_0)} \\
\sqrt{(1-\alpha c_0)(1-\alpha)} \\
0 \\
0
\end{pmatrix},
&
\begin{pmatrix}
\sqrt{\alpha^2 c_0} \\
\sqrt{\alpha^2 (1-c_0)} \\
\sqrt{\alpha(1-\alpha)c_0} \\
\sqrt{\alpha(1-\alpha)c_0} \\
\sqrt{(1+\alpha-2\alpha c_0)(1-\alpha)} \\
0 \\
0 \\
0
\end{pmatrix},
&
\begin{pmatrix}
\sqrt{\alpha^2 c_0} \\
\sqrt{\alpha^2 (1-c_0)} \\
\sqrt{\alpha(1-\alpha)c_0} \\
\sqrt{(1-\alpha^2)/2} \\
\sqrt{(1+\alpha-2\alpha c_0)(1-\alpha)/2} \\
0 \\
0 \\
0
\end{pmatrix}.
\end{array}
\tag{B5}
$$

The kth T transform, $T_{i,j}^{(k)}$, involves unitaries and generalized measurements on the 2×2 subspace $(|i\rangle_A, |j\rangle_A)$ of $\mathcal{H}^{a_1} \otimes \mathcal{H}^{a_2} \otimes \mathcal{H}^{a_3}$ and the corresponding subspace $(|i\rangle_B, |j\rangle_B)$ of $\mathcal{H}^{b_1} \otimes \mathcal{H}^{b_2} \otimes \mathcal{H}^{b_3}$. The transformation $|I\rangle \rightarrow |I_1\rangle$ is implemented using the following steps. First, Alice (agent at A) and Bob (agent at B) apply the local unitaries on the $\{|7\rangle_A, |8\rangle_A\}$ and $\{|7\rangle_B, |8\rangle_B\}$ subspaces, respectively,

$$
U_A^{(1)} = \begin{pmatrix} 1/\sqrt{2} & 1/\sqrt{2} \\ 1/\sqrt{2} & -1/\sqrt{2} \end{pmatrix}, \quad U_B^{(1)} = \begin{pmatrix} \sqrt{c_0} & \sqrt{1-c_0} \\ \sqrt{1-c_0} & -\sqrt{c_0} \end{pmatrix}.
\tag{B6}
$$

Alice then performs a generalized measurement using the following operators on the $\{|7\rangle_A, |8\rangle_A\}$ space:

$$
M_{A,1}^{(1)} = \frac{\mathbb{1}_{A\backslash\{7,8\}}}{\sqrt{2}} \oplus |7\rangle_A \langle 7|,
$$

$$
M_{A,2}^{(1)} = \frac{\mathbb{1}_{A\backslash\{7,8\}}}{\sqrt{2}} \oplus |8\rangle_A \langle 8|,
\tag{B7}
$$

which form a complete set of measurements for Alice's systems since $(M_{A,1}^{(1)})^\dagger M_{A,1}^{(1)} + (M_{A,2}^{(1)})^\dagger M_{A,2}^{(1)} = \mathbb{1}_A$. The measurement result is then communicated to Bob who applies $\mathbb{1}_B$ in the case in which Alice obtains $m_1^{(1)}$ and applies $\tilde{U}_B^{(1)}$ on the $\{|7\rangle_B, |8\rangle_B\}$ subspace if $m_2^{(1)}$ is obtained where [with $\cos\gamma_1 = (2c_0 - 1)$]

$$
\tilde{U}_B^{(1)} = \begin{pmatrix} \cos\gamma_1 & \sin\gamma_1 \\ \sin\gamma_1 & -\cos\gamma_1 \end{pmatrix}.
\tag{B8}
$$

The transformation $|I_1\rangle \rightarrow |I_2\rangle$ is implemented similarly by first applying local unitary transforms at Alice and Bob's stations,

$$
U_A^{(2)} = \begin{pmatrix} 1/\sqrt{2} & 1/\sqrt{2} \\ 1/\sqrt{2} & -1/\sqrt{2} \end{pmatrix}, \quad U_B^{(2)} = \begin{pmatrix} \sqrt{s} & \sqrt{1-s} \\ \sqrt{1-s} & -\sqrt{s} \end{pmatrix}
\tag{B9}
$$

with $s = \alpha(1-c_0)/(1-\alpha c_0)$. This is followed by the measurement of local operators by Alice,

$$
M_{A,1}^{(2)} = \frac{\mathbb{1}_{A\backslash\{6,7\}}}{\sqrt{2}} \oplus |6\rangle_A \langle 6|,
$$

$$
M_{A,2}^{(2)} = \frac{\mathbb{1}_{A\backslash\{6,7\}}}{\sqrt{2}} \oplus |7\rangle_A \langle 7|,
\tag{B10}
$$

and the measurement results communicated to Bob. If Alice obtains $m_1^{(2)}$, Bob applies $\mathbb{1}_B$, and if Alice obtains $m_2^{(2)}$, then

Bob applies [with $\cos\gamma_2 = [2\alpha - (1+\alpha c_0)]/(1-\alpha c_0)$]

$$
\tilde{U}_B^{(2)} = \begin{pmatrix} \cos\gamma_2 & \sin\gamma_2 \\ \sin\gamma_2 & -\cos\gamma_2 \end{pmatrix}.
\tag{B11}
$$

The transformation $|I_2\rangle \rightarrow |I_3\rangle$ is implemented similarly by first applying local unitary transforms at Alice and Bob's stations,

$$
U_A^{(3)} = \begin{pmatrix} 1/\sqrt{2} & 1/\sqrt{2} \\ 1/\sqrt{2} & -1/\sqrt{2} \end{pmatrix}, \quad U_B^{(3)} = \begin{pmatrix} \sqrt{s} & \sqrt{1-s} \\ \sqrt{1-s} & -\sqrt{s} \end{pmatrix},
\tag{B12}
$$

with $s = \alpha(1-c_0)/(1+\alpha-2\alpha c_0)$. This is followed by the measurement of local operators by Alice,

$$
M_{A,1}^{(3)} = \frac{\mathbb{1}_{A\backslash\{5,6\}}}{\sqrt{2}} \oplus |5\rangle_A \langle 5|,
$$

$$
M_{A,1}^{(3)} = \frac{\mathbb{1}_{A\backslash\{5,6\}}}{\sqrt{2}} \oplus |6\rangle_A \langle 6|,
\tag{B13}
$$

and the measurement results communicated to Bob. If Alice obtains $m_1^{(3)}$, Bob applies $\mathbb{1}_B$, and if Alice obtains $m_2^{(3)}$, then Bob applies [with $\cos\gamma_3 = (\alpha - 1)/(1+\alpha-2\alpha c_0)$]

$$
\tilde{U}_B^{(3)} = \begin{pmatrix} \cos\gamma_3 & \sin\gamma_3 \\ \sin\gamma_3 & -\cos\gamma_3 \end{pmatrix}.
\tag{B14}
$$

The transformation $|I_3\rangle \rightarrow |I_4\rangle$ is implemented similarly by first applying local unitary transforms at Alice and Bob's stations,

$$
U_A^{(4)} = \begin{pmatrix} 1/\sqrt{2} & 1/\sqrt{2} \\ 1/\sqrt{2} & -1/\sqrt{2} \end{pmatrix}, \quad U_B^{(4)} = \begin{pmatrix} \sqrt{s} & \sqrt{1-s} \\ \sqrt{1-s} & -\sqrt{s} \end{pmatrix},
\tag{B15}
$$

with $s = \alpha c/(1+\alpha-\alpha c)$. This is followed by the measurement of local operators by Alice,

$$
M_{A,1}^{(4)} = \frac{\mathbb{1}_{A\backslash\{4,5\}}}{\sqrt{2}} \oplus \cos\delta |4\rangle_A \langle 4| + \sin\delta |5\rangle_A \langle 5|,
$$

$$
M_{A,2}^{(4)} = \frac{\mathbb{1}_{A\backslash\{4,5\}}}{\sqrt{2}} \oplus \sin\delta |4\rangle_A \langle 4| + \cos\delta |5\rangle_A \langle 5|,
\tag{B16}
$$

with $\cos\delta = \{0.5 + 0.5\sqrt{[4\alpha c_0 - (1+\alpha)]/(4\alpha c_0)}\}^{1/2}$ and the measurement results communicated to Bob. If Alice obtains $m_1^{(4)}$, Bob applies $\mathbb{1}_B$, and if Alice obtains $m_2^{(4)}$, then Bob

applies [with $\cos \gamma_4 = (3\alpha c_0 - 1 - \alpha)/(1 + \alpha - \alpha c_0)$]

$$\tilde{U}_B^{(4)} = \begin{pmatrix} \cos \gamma_4 & \sin \gamma_4 \\ \sin \gamma_4 & -\cos \gamma_4 \end{pmatrix}. \tag{B17}$$

Next, the transformation $|I_4\rangle \to |\gamma_1\rangle$ is implemented by first applying local unitary transforms at Alice and Bob's stations,

$$U_A^{(5)} = \begin{pmatrix} 1/\sqrt{2} & 1/\sqrt{2} \\ 1/\sqrt{2} & -1/\sqrt{2} \end{pmatrix}, \quad U_B^{(5)} = \begin{pmatrix} \sqrt{s} & \sqrt{1-s} \\ \sqrt{1-s} & -\sqrt{s} \end{pmatrix}, \tag{B18}$$

with $s = 2\alpha c_0/(1 + \alpha)$. This is followed by the measurement of local operators by Alice,

$$M_{A,1}^{(5)} = \frac{\mathbb{1}_{A\setminus\{3,5\}}}{\sqrt{2}} \oplus |3\rangle_A \langle 3|,$$

$$M_{A,2}^{(5)} = \frac{\mathbb{1}_{A\setminus\{3,5\}}}{\sqrt{2}} \oplus |5\rangle_A \langle 5|, \tag{B19}$$

and the measurement results communicated to Bob. If Alice obtains $m_1^{(5)}$, Bob applies $\mathbb{1}_B$, and if Alice obtains $m_2^{(5)}$, then Bob applies [with $\cos \gamma_5 = [(4\alpha c_0)/(1 + \alpha) - 1]$],

$$\tilde{U}_B^{(5)} = \begin{pmatrix} \cos \gamma_5 & \sin \gamma_5 \\ \sin \gamma_5 & -\cos \gamma_5 \end{pmatrix}. \tag{B20}$$

This completes the process of deterministically obtaining the shared state $|\gamma\rangle$ between A and B using local operations and multiple rounds of one-way classical communication.

The sequence of operations (B6)–(B20) can, however, be equivalently performed by completing all operations on Alice's side first and then communicating five bits of classical data to Bob which determines the unitary that Bob applies. For this, the generalized measurements (B7), (B10), (B13), (B16), and (B19) are performed by unitarily interacting qubits a_1, a_2, a_3 with measurement qubits $q^{(i)}$, initialized in the $|0\rangle$ state, via unitaries $U_{A,M}^{(i)}$, respectively, where

$$U_{A,M}^{(1)} = \frac{\mathbb{1}_{A\setminus\{7,8\}}}{\sqrt{2}} \otimes (HX) + |7\rangle \langle 7| \otimes \mathbb{1} + |8\rangle \langle 8| \otimes iY, \tag{B21}$$

$$U_{A,M}^{(2)} = \frac{\mathbb{1}_{A\setminus\{6,7\}}}{\sqrt{2}} \otimes (HX) + |6\rangle \langle 6| \otimes \mathbb{1} + |7\rangle \langle 7| \otimes iY, \tag{B22}$$

$$U_{A,M}^{(3)} = \frac{\mathbb{1}_{A\setminus\{5,6\}}}{\sqrt{2}} \otimes (HX) + |5\rangle \langle 5| \otimes \mathbb{1} + |6\rangle \langle 6| \otimes iY, \tag{B23}$$

$$U_{A,M}^{(4)} = \frac{\mathbb{1}_{A\setminus\{4,5\}}}{\sqrt{2}} \otimes (HX) + |4\rangle \langle 4| \otimes (\cos \delta \mathbb{1} + \sin(\delta)iY)$$
$$+ |5\rangle \langle 5| \otimes [\sin \delta \mathbb{1} + \cos(\delta)iY], \tag{B24}$$

$$U_{A,M}^{(5)} = \frac{\mathbb{1}_{A\setminus\{3,5\}}}{\sqrt{2}} \otimes (HX) + |3\rangle \langle 3| \otimes \mathbb{1} + |5\rangle \langle 5| \otimes iY, \tag{B25}$$

where $\cos \delta = \{0.5 + 0.5\sqrt{[4\alpha c_0 - (1 + \alpha)]/(4\alpha c_0)}\}^{1/2}$. The measurement qubits are then measured in the computational basis to obtain five bits of classical data, $\bar{m}_A \in \{0, 1\}^5$. The complete sequence of unitaries applied by Alice is therefore (with the earlier unitary, i.e., with smaller "i," to the right)

$$\prod_{i=1}^{i=5} U_{A,M}^{(i)} U_A^{(i)}. \tag{B26}$$

The five bits of classical data is then conveyed to Bob which determines the unitary that it applies to qubits b_1, b_2, b_3,

$$U_B(\alpha, c, \bar{m}_A) = \prod_{i=1}^{i=5} \left(\tilde{U}_B^{(i)}\right)^{m_{A,i}} U_B^{(i)}. \tag{B27}$$

The quantum circuit for each pair of unitaries $U_{A,M}^{(i)} U_A^{(i)}$ in expression (B26) has an approximate depth of 20. Step two as described in the main text involves Bob measuring the operators on qubits b_1, b_2, b_3,

$$M_{B,1} = \cos \kappa_1 |1\rangle_B \langle 1| + \cos \kappa_2 |2\rangle_B \langle 2| + \mathbb{1}_{A\setminus\{1,2\}},$$

$$M_{B,2} = \sin \kappa_1 |1\rangle_B \langle 1| + \sin \kappa_2 |2\rangle_B \langle 2| \tag{B28}$$

where $\cos \kappa_1 = \sqrt{(1 - \alpha^2)/[2\alpha^2(1 - c_0)]}$ and $\cos \kappa_2 = \sqrt{[c_0(1 - \alpha^2)]/[2\alpha^2(1 - c_0)^2]}$. If the outcome of Bob's measurement is m_1 corresponding to $M_{B,1}$, then they obtain the postmeasurement state $|\beta\rangle \otimes |\mathcal{C}_0\rangle \otimes |HV\rangle$ with probability $P(\alpha) = (1 - \alpha^2)/[1 - c_0(2, \alpha)]$. On the other hand, if Bob obtains m_2, then the attempt has been a failure. In either case the outcome is conveyed to Alice so that subsequent actions for long-range entanglement distribution can continue.

---

[1] S. Wehner, D. Elkouss, and R. Hanson, Quantum internet: A vision for the road ahead, Science **362**, eaam9288 (2018).

[2] J. Yin, Yu-Huai Li, Sheng-Kai Liao, M. Yang, Y. Cao, L. Zhang, Ji-Gang Ren, Wen-Qi Cai, Wei-Yue Liu, Shuang-Lin Li *et al.*, Entanglement-based secure quantum cryptography over 1,120 kilometres, Nature (London) **582**, 501 (2020).

[3] W. Rosenfeld, D. Burchardt, R. Garthoff, K. Redeker, N. Ortegel, M. Rau, and H. Weinfurter, Event-Ready Bell Test Using Entangled Atoms Simultaneously Closing Detection and Locality Loopholes, Phys. Rev. Lett. **119**, 010402 (2017).

[4] P. Kómár, E. M. Kessler, M. Bishof, L. Jiang, A. S. Sorensen, J. Ye, and M. D. Lukin, A quantum network of clocks, Nat. Phys. **10**, 582 (2014).

[5] E. T. Khabiboulline, J. Borregaard, K. De Greve, and M. D. Lukin, Optical Interferometry with Quantum Networks, Phys. Rev. Lett. **123**, 070504 (2019).

[6] B. T. Kirby, S. Santra, V. S. Malinovsky, and M. Brodsky, Entanglement swapping of two arbitrarily degraded entangled states, Phys. Rev. A **94**, 012336 (2016).

[7] W. J. Munro, K. Azuma, K. Tamaki, and K. Nemoto, Inside quantum repeaters, IEEE J. Sel. Top. Quantum Electron. **21**, 78 (2015).

[8] P. G. Kwiat, S. Barraza-Lopez, A. Stefanov, and N. Gisin, Experimental entanglement distillation and 'hidden' non-locality, Nature (London) **409**, 1014 (2001).

[9] Jian-Wei Pan, S. Gasparoni, R. Ursin, G. Weihs, and A. Zeilinger, Experimental entanglement purification of arbitrary unknown states, Nature (London) **423**, 417 (2003).

[10] L. Gyongyosi and S. Imre, Dynamic topology resilience for quantum networks, in *Advances in Photonics of Quantum Computing, Memory, and Communication XI*, edited by Zameer Ul Hasan, Philip R. Hemmer, Alan E. Craig, and Alan L. Migdall, International Society for Optics and Photonics (SPIE, Bellingham, WA, 2018), Vol. 10547, pp. 89–95.

[11] Yi-Han Luo, Han-Sen Zhong, M. Erhard, Xi-Lin Wang, Li-Chao Peng, M. Krenn, X. Jiang, L. Li, Nai-Le Liu, Chao-Yang Lu *et al.*, Quantum Teleportation in High Dimensions, Phys. Rev. Lett. **123**, 070505 (2019).

[12] W. Kozlowski and S. Wehner, Towards large-scale quantum networks, in *Proceedings of the Sixth Annual ACM International Conference on Nanoscale Computing and Communication (NANOCOM '19)* (Association for Computing Machinery, New York, NY, 2019).

[13] D. Jonathan and M. B. Plenio, Entanglement-Assisted Local Manipulation of Pure Quantum States, Phys. Rev. Lett. **83**, 3566 (1999).

[14] M. A. Nielsen, Conditions for a Class of Entanglement Transformations, Phys. Rev. Lett. **83**, 436 (1999).

[15] G. Vidal, Entanglement of Pure States for a Single Copy, Phys. Rev. Lett. **83**, 1046 (1999).

[16] S. Santra and V. S. Malinovsky, Catalyzed entanglement concentration of qubit pairs, arXiv:2007.10516.

[17] G. R. Walsh, *An Introduction to Linear Programming* (Wiley, New York, 1985).

[18] J. Eisert and M. Wilkens, Catalysis of Entanglement Manipulation for Mixed States, Phys. Rev. Lett. **85**, 437 (2000).

[19] D. E. Jones, B. T. Kirby, and M. Brodsky, Tuning quantum channels to maximize polarization entanglement for telecom photon pairs, npj Quantum Inf. **4**, 58 (2018).

[20] R. A. Brewster, B. T. Kirby, J. D. Franson, and M. Brodsky, Compensation of polarization-dependent loss using noiseless amplification and attenuation, Phys. Rev. A **100**, 033811 (2019).

[21] A. Dumenil, Polarization dependent loss in next-generation optical networks: Challenges and solutions, HAL archives (2020).

[22] M. Brekenfeld, D. Niemietz, J. D. Christesen, and G. Rempe, A quantum network node with crossed optical fibre cavities, Nat. Phys. **16**, 647 (2020).

[23] For P small, $Z^{(N)}(P) \approx 1/[P(2/3)^{N-1}]$, which is the case for both $P_{cat}^{max}(n, \alpha, c_0)$ and $P_{LOCC}^{max}(n, \alpha)$ as $\alpha \to 1$.

[24] N. K. Bernardes, L. Praxmeyer, and P. van Loock, Rate analysis for a hybrid quantum repeater, Phys. Rev. A **83**, 012323 (2011).

[25] R. F. Werner, Quantum states with Einstein-Podolsky-Rosen correlations admitting a hidden-variable model, Phys. Rev. A **40**, 4277 (1989).

[26] P. W. Shor, Capacities of quantum channels and how to find them, Math. Program. **97**, 311 (2003).

[27] J. Wallnöfer, M. Zwerger, C. Muschik, N. Sangouard, and W. Dür, Two-dimensional quantum repeaters, Phys. Rev. A **94**, 052307 (2016).